WILEY-VCH

COMMUNICATION

An Organic-Inorganic Hybrid Cathode Based on S-Se Dynamic Covalent Bonds

Jiawei Zhao,†[a] Yubing Si,†[a] Zixiao Han,[a] Junjie Li,[b] Wei Guo,[a] and Yongzhu Fu*[a]

Abstract: *Organic-inorganic hybrid cathode materials have advantages of both components. Herein, we report an attractive diphenyl trisulfide-selenium nanowire (DPTS-Se) hybrid cathode material for rechargeable lithium batteries. During discharge, three voltage plateaus associated with three lithiation processes are observed. During recharge, the combination of the radicals formed upon delithiation leads to several new phenyl sulfoselenide compounds which are confirmed by HPLC-QTof-MS. The formation of S-Se dynamic covalent bonds is further investigated computationally. Thus, the redox process of DPTS-Se is clearly revealed. The hybrid cathode exhibits superior cycling stability over pristine Se or DPTS as cathode alone. The first discharge shows a capacity of 96.5% of the theoretical specific capacity and the cell retains 69.2% of the initial capacity over 250 cycles. The hybrid cathode also shows a high Coulombic efficiency of over 99% after 250 cycles. This study demonstrates that the combination of organic polysulfide and selenium can not only improve the utilization of active materials but also enhance the cycling performance. Accordingly, such organic-inorganic hybrid material is a unique system for fundamental understanding and potential application in high-energy density batteries.*

Lithium-ion (Li-ion) batteries have the advantage of high energy densities,[1] therefore they are widely used in portable electronics. However, the current cathode materials such as $LiCoO_2$ and $LiFePO_4$ have reached their capacity limits. Discovering revolutionary cathode materials with high energy density is one of the crucial challenges in energy research. Organic compounds offer new possibilities for high energy density, high capacity, and multifunctional molecule design.[2] Some organic polysulfide molecules with high capacities, such as dimethyl trisulfide,[3] diphenyl trisulfide (DPTS), diphenyl tetrasulfides,[4] and stretchable polymers,[5] have been investigated and they show promising electrochemical performance in lithium batteries. For example, organic polysulfides can avoid the formation of high-order lithium polysulfides upon cycling, helping them to overcome the issues of shuttle effect. The diverse structures of organic electrode materials allow intriguing redox reactions to occur. But they have the disadvantage of poor cycling and low rate performance due to their high solubility in liquid electrolytes and low conductivity.

The popular cathode candidate, selenium (Se), is promising as it has a high theoretical specific capacity of 679 mAh g^{-1}. Upon discharge in lithium batteries, lithium polyselenides are formed, which result in shuttle effect in the following charge. It shows unsatisfactory battery performance when used alone. Several strategies have been developed to overcome these issues such as using microporous carbon hosts.[6] One interesting approach is to utilize Se_xS_y hybrids as cathode materials.[7] The S-Se bonds in Se_xS_y lead to alternative reduction pathways and discharge products,[7c,8] and good cycling performance in lithium batteries.[9] Besides inorganic SeS_2 compounds, our group reported diphenyl selenosulfide (PhS-SePh) having a S-Se bond as a cathode material,[10] which shows higher discharge voltage and better cycling stability than diphenyl disulfide (DPDS) and diselenide. Accordingly, compounds containing S-Se bonds not only provide opportunities for fundamental understanding of redox reactions, but also have the potential to enable high performance rechargeable lithium batteries. To have the excellent properties of organic polysulfide, selenium, and S-Se bonds, a subtle approach is to develop organic-inorganic hybrid materials containing conductive Se and functional organic polysulfide.[11]

Herein, we report a DPTS-Se hybrid cathode for rechargeable lithium batteries, as shown in **Figure 1A**. Se nanowires were synthesized by a facile method,[12] then mixed with carbon nanotubes to form a self-weaving composite electrode. DPTS introduced in the electrode is a promising organic polysulfide material with a theoretical capacity of 428 mAh g^{-1}. The mixture of organic DPTS and inorganic Se is expected to generate new redox processes involving S-Se bonds, enhance the specific capacity and cycling stability. Electrochemical and material characterization techniques have been used to understand the redox reactions of DPTS-Se in lithium cells. Density functional theory (DFT) and Born-Oppenheimer molecular dynamics (BOMD) approaches have been employed to simulate the formation of dynamic S-Se covalent bonds in the charge process.

The DPTS-Se hybrid electrode is prepared by a two-step method.[13] First, selenium oxide (SeO_2) and beta–cyclodextrin (β–cyclodextrin) were dissolved in de-ionized water to generate selenium nanowires with the assistance of ascorbic acid. A certain proportion of selenium nanowires and CNTs were dispersed in an ethyl alcohol mixture. After vigorous agitation and ultrasonication, the selenium nanowires and CNTs were self-woven, then filtered and dried in a vacuum drying oven at 35 °C for 24 h. The detailed process description is given in **Figure S1** in the supporting information. The scanning electron microscopy (SEM) image reveals that the Se nanowires are imbedded in the CNT network, as shown in **Figure S2**. The Se/CNT composite electrode is highly porous and the electrode can be made in large area. Without binder, the composite electrode is highly conductive, which can enable high utilization of active material. The crystal structure and phase of the as-prepared Se/CNT composite electrode are examined by X-ray diffraction (XRD). As shown in **Figure 1B**, several peaks at 23.51 (100), 29.71 (101), 41.31 (110), 43.61 (102), 45.41 (111), 51.81 (201), 55.71 (112), and 61.51 (202) are in good agreement with the diffraction peaks of Se, which are indexed to hexagonal Se (JCPDS 06-0362), indicating that pure Se has been prepared. The inset transmission electron microscopy (TEM) image shows the Se nanowires are straight and have a diameter of *ca.* 100 nm. The Brunauer–Emmett–Teller

[a] J. Zhao, Dr. Y. Si, Z. Han, Profs. W. Guo and Y. Fu
College of Chemistry
Zhengzhou University
Zhengzhou 450001, P. R. China
E-mail: yfu@zzu.edu.cn (Y. Fu)
[b] Dr. J. Li
Research Technologies, Indiana University, Indianapolis, IN 46202, U. S. A.
† These authors contribute equivalently.

10.1002/anie.201913243

specific surface area of the Se/CNT composite electrode calculated from the N_2 sorption isotherms (**Figure S3**) is 123.08 m^2 g^{-1}. The pore size distribution is centered at around 2.84 nm, and the adsorption average pore width is 22.50 nm.

When the DPTS catholyte is added, it is immediately adsorbed by the Se/CNTs composite electrode. The DPTS:Se molar ratio is 1:1. The hybrid cathode prepared in this manner allows Se and DPTS to be physically trapped within the CNT network, reducing dissolution of the discharge products and inhibiting the shuttle effect.[14] As shown in **Figures S4**, the sulfur element (*i.e.*, DPTS) is uniformly distributed in the Se/CNTs composite electrode. The electrochemical performance of the DPTS-Se hybrid cathode is evaluated in Li half cells. The initial discharge-charge voltage profile of a Li/DPTS-Se cell is shown in **Figure 1C**. It can be seen that a slope voltage region at about 2.30 V appears during the first discharge, which is probably due to the formation PhSSLi,[4a] PhSLi, and Li_2Se_8. In the following process, the DPTS-Se cathode exhibits two discharge plateaus at 2.05 and 1.95 V,[15] which are attributed to the formation of Li_2S and Li_2Se. For comparison, the discharge/charge profiles of Se and DPTS cathodes are also shown in **Figure 1C**. The Se electrode exhibits standard two discharge voltage regions at 2.15 V and 2.02 V. The DPTS electrode shows a voltage slope and plateau. Clearly, the DPTS-Se hybrid electrode has the voltage characteristics of both Se and DPTS materials. However, the initial discharge capacity (2.38 mAh) of the DPTS-Se electrode is higher than the sum of the Se (0.89 mAh) and DPTS (1.15 mAh). The charge voltage profiles are mainly increasing slopes for all the three cells. The Li/DPTS-Se cell exhibits a high energy efficiency of 95.8%. After recharge, the DPTS-Se electrode exhibits strong crystalline peaks of Se as shown in **Figure 1D**, indicating elemental Se is still reformed although the peak intensities are different from those of the starting Se nanowires. In addition, the morphology of the hybrid electrode is completely different, as shown in the inset in **Figures 1D** and **S5**. Se nanowires are converted to nanocrystals which are intimately composited with CNTs.

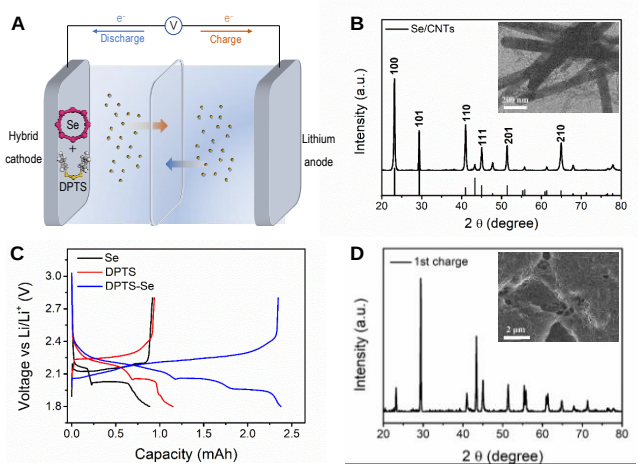

Figure 1. (**A**) A schematic lithium half cell with DPTS-Se hybrid cathode. (**B**) XRD pattern of the fresh Se/CNT composite, the inset is TEM image of the composite. (**C**) The first discharge and recharge voltage profiles of Li/Se, Li/DPTS, and Li/DPTS-Se cells. (**D**) XRD pattern of the recharged DPTS-Se electrode, the inset is SEM image of the electrode.

The improved battery performance of the DPTS-Se hybrid electrode indicates alternative redox reaction mechanisms. The charged products, ultra-high performance liquid chromatography-quadrupole time-of-flight-mass spectrometry (UPLC-QToF-MS) was used, which has been proved to be a powerful tool for the identification of trace constituents of complex mixtures. A solvent-extraction from the electrode was detected by Waters Xevo G2XS QTof mass spectrometer fitted with an ESI source. The m/z of the target analyte is extracted from the total ion chromatograms (TICs) and the accurate mass of the compound was obtained. Precise mass spectrometry analyses of the components separated in the LC-QToF-MS system is analyzed using the QToF-MS function. **Figures 2A-D** display the most characteristic fragments obtained from the $[M-H]^-$ ions of all the components, which are noted by their m/z values. The ESI-MS spectra present four types of negatively protonated molecular ions with m/z values of 298.973, 330.944, 377.317, and 458.772, corresponding to PhSSeSPh, PhSSeSSPh, PhSSeSeSPh, and PhSSeSeSeSPh, respectively. It can be seen that some Se atoms are inserted in the molecular structures of DPDS and DPTS in the charge process, which can reduce the formation of lithium polyselenides such as Li_2Se_8 thus improve the cycling stability.

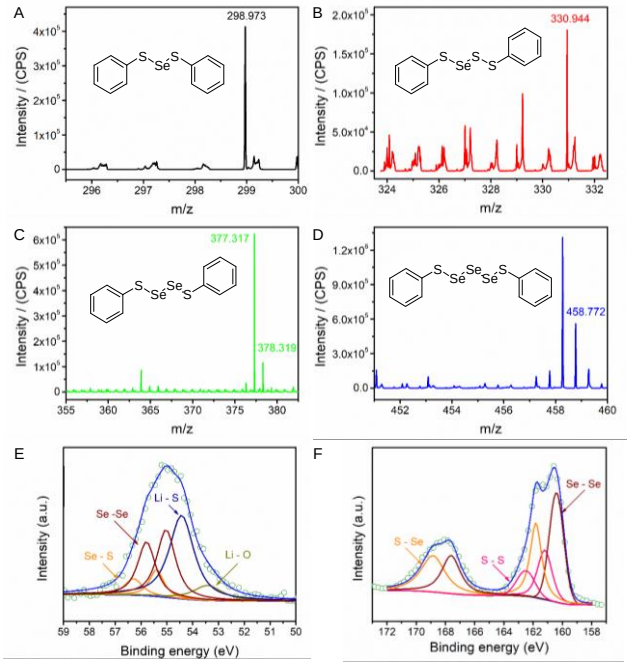

Figure 2. Total ion chromatograms and XPS spectra of a DPTS-Se electrode after charge. The mass spectra of the charged products: (**A**) PhSSeSPh, (**B**) PhSSeSSPh, (**C**) PhSSeSeSPh, and (**D**) PhSSeSeSeSPh. (**E**) and (**F**) XPS spectra.

The presence of S-S and S-Se bonds in the charged products is characterized by Raman spectroscopy and X-ray photoelectron spectroscopy (XPS). Raman spectrum of the charged product of the DPTS-Se hybrid electrode is shown in **Figure S6**. The peak near 470 cm^{-1} is assigned to S-S stretching vibration.[16] There are some small peaks around 350 cm^{-1}, which are assigned to Se-S stretching vibrations.[7a, 17] XPS data further ascertain the chemical composition and the chemical bonding state. As shown

10.1002/anie.201913243

in **Figure S7**, the Se $3d_{5/2}$ and $3d_{3/2}$ peaks of the fresh Se-CNTs electrode are found at 55.31 and 56.17 eV.[18] While the charged DPTS-Se electrode displays two major peaks at 55.02 and 55.85 eV, corresponding to Se $3d_{5/2}$ and Se $3d_{3/2}$, respectively, as shown in **Figure 2E**. In addition, a new doublet at a higher binding energy of 55.39/56.28 eV in the Se 3d spectrum are assigned to Se bonded to S (heteropolar Se-S bond).[19] Meanwhile, there are two major doublets at 161.20/162.48 and 160.40/167.60 eV correspond to S bonded to S (homopolar S-S bonds) and Se bonded to Se (homopolar Se-Se bonds), as shown in **Figure 2F**. While the two new doublets at 161.81/168.85 eV are assigned to Se bonded to S (S-Se bonds).[8] According to the XPS analysis, the predominant peaks of Se 3d exist. Meanwhile, the presence of S-Se and S-S bonds are also confirmed by the XPS data.

To get deeper understanding of the reaction mechanisms and reveal the relationship between dynamic covalent S-Se bonds and their properties, the charging process was simulated by density functional theory (DFT) and Born-Oppenheimer molecular dynamics (BOMD) model. Considering that in the selenium-rich system, the fragment of PhS• radical would preferably break a Se-Se bond, and results in the formation of S-Se bond in the organic species,[17] our computational study was carried out in two steps.

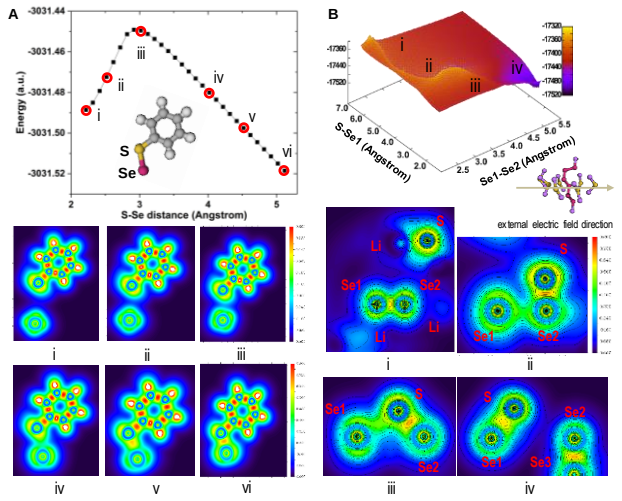

Figure 3. (**A**) The total potential energy of Se atom and C_6H_5S• radical along the reaction coordinate (S-Se distance) and the selected six snapshots. (**B**) The potential energy surface of Li_2Se_6 reacts with seven Li_2S and the spin density plots for the four snapshots.

Firstly, DFT calculation at M062X/cc-pVTZ level was used to scan the reaction coordinate to simulate PhS• radical attacking a Se atom. An external electric field was applied along the Y-axis (parallel the S-Se bond) with the intensity of 0.02 a.u. (about 1V/Å). In **Figure 3A**, it is clear to see that the S-Se covalent bond formed gradually along the reaction coordinate, while the Mulliken charge analysis shows that the electron keeps transfer from PhS• radical to Se, which is consistent with the XPS results. Then, BOMD simulations of Se-S and Se-Se bonds in the inorganic intermediates is further performed to gain insights into the mechanism of bonds cleavage and formation. The binary complex of one Li_2Se_6 with seven Li_2S were simulated at the B3LYP/6-31G(d) level to balance the accuracy and speed. The yielded 5000 snapshots and the corresponding potential energy surface (PES) of the delithiation process along the cleavage of Se-Se and formation of Se-S bond was shown in **Figure 3B**. Driven by the external electron field, the delithiation process is very quick, 2/3 lithium atoms are released from Li_2Se_6 and Li_2S in less than 400 fs. It is worth noting that the total potential energy is decreasing when the distance of Se1 (the first selenium atom) and S bond is getting closer during the charging stage, meantime, a charge transfer is observed from the S to Se1 atom followed by a weak S-Se bond formed. The formation of this bond reduces the dissolution loss of polyselenide and polysulfide during the charge process and achieves the fixation at the atomic level. It fits well with the experiment observation and DFT calculations.

From the analysis of the charged products and results from literature, we can formulate the redox reactions of the organic-inorganic DPTS-Se hybrid electrode in lithium batteries, as simply elaborated in **Figure 4**. In the 1st discharge process, the S-S bonds in DPTS could undergo cleavage into PhS• and PhSS• due to favorable kinetics and stabilization. These radicals react with Li^+ and e^- to form PhSLi and PhSSLi. In the following, elemental selenium is lithiated to form lithium polyselenides such as Li_2Se_8. The formation of PhSSLi and Li_2Se_8 corresponds to the first discharged plateau. PhSSLi is formed in the first half and Li_2Se_8 is formed in the second half stages. The cyclic voltammograms in **Figure S8** clearly show the overlapped cathodic peaks at 2.1 and 2.0 V. PhSSLi is further reduced to PhSLi and Li_2S, which leads to the second voltage plateau. Polyselenides are converted to Li_2Se corresponding to the third plateau. PhSLi, Li_2S, and Li_2Se are the primary discharge products. In the recharge process, diversified products are formed due to the cleavage of bonds and different combinations of free radicals upon delithiation. First, Li_2Se, Li_2S, and PhSLi are delithiated, which could result in •Se•, •S•, PhS• radicals. They are combined individually or in pairs to form new products that are not limited to the starting material. Some selenium radicals are converted to crystalline selenium in the final charge. The formation of S-Se bonds is believed to be highly dynamic involving rapid reconfiguration. In the following discharge, these new diphenyl sulfoselenide compounds undergo reduction reactions. Due to the similar electron configuration between sulfur and selenium, these compounds show similar discharge voltage plateaus as the starting materials (as shown in Figure 5).

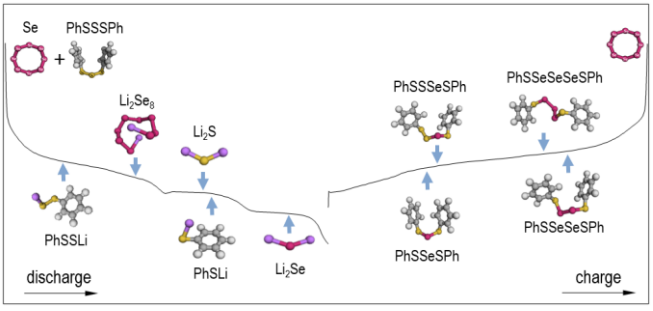

Figure 4. The redox reactions of the DPTS-Se cathode in a lithium cell.

Figure 5A shows the cycling performance of a Li/DPTS-Se cell. A high initial discharge capacity of 471.1 mAh g^{-1} is obtained at 0.1 C rate, which is 96.5% of the theoretical capacity of all the active material in the electrode. The DPTS-Se cathode shows excellent cycling stability and retains a specific capacity of 325.8

mAh g^{-1} after 250 cycles. The capacity retention is 69.2% as shown in the inset. We also evaluated the Se/CNTs electrode to identify the capacity contribution from Se and CNTs in the composite electrode. The Li/Se cell shows low capacities and poor cycle stability in **Figure S9**. The initial discharge capacity is 820.7 mAh g^{-1} at 0.1 C rate and the capacity after 200 cycles is 128.3 mAh g^{-1}. The capacity fading in the Se cathode is probably induced by the dissolution and diffusion of lithium polyselenides into the ether-based electrolyte. The comparison confirms the enhancement of the cycling stability due to the alternative redox reaction process in the DPTS-Se cathode reducing the loss of active material. The Li/DPTS control cell was also evaluated. **Figure S10** shows the actual capacities of Se and DPTS from the Li/Se and Li/DPTS control cells. **Figure S11** compares the sum of the capacities of Se and DPTS from the control cells and capacities of DPTS-Se from the Li/DPTS-Se cell. The comparison indicates the hybrid cathode performs much better than the components when they work alone in the aspect of material utilization. In addition, the hybrid cathodes with different DPTS:Se molar ratios were also evaluated. The DPTS:Se molar ratio affects the cycling performance because the mass loading and active material:carbon ration in the composite electrodes are different (**Figure S12**). **Figure 5B** shows some selected voltage profiles. From the 1st to 50th cycle, each voltage plateau decreases. Afterwards, the capacity decrease is mainly due to the shrinkage of the third plateau at 1.95 V, indicating continuous loss of Se. However, it is worth noting that the two high discharge voltage plateaus almost do not change. In another word, the formed diphenyl sulfoselenide compounds (*e.g.*, PhSSeSPh, PhSSeSSPh, PhSSeSeSPh, and PhSSeSeSeSPh) in the hybrid electrode remain constant after the first 50 cycles. This result indicates that the Se atoms fixed in the molecular structures of diphenyl sulfoselenide compounds and inorganic intermediates can remain electrochemically stable over prolonged cycles. This phenomenon is also confirmed from the XRD data presented in **Figure S13**. In the 200th and 250th cycles, the Se diffraction peaks weaken significantly, meaning most crystalline selenium is converted to amorphous species. Therefore, the retention of capacity benefits from the formation of S-Se dynamic covalent bonds, which enable a molecular level fixation effect on selenium atoms in the DPTS-Se hybrid cathode. The DPTS-Se electrode exhibits good rate capability, as shown in **Figure S14**. The cell shows capacities of over 200 mAh g^{-1} at 1C rate.

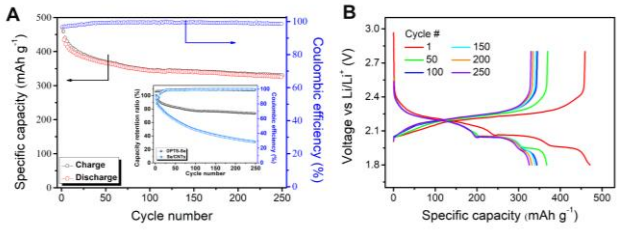

Figure 5. (**A**) Cycling performance and Coulombic efficiency of a Li/DPTS-Se cell at 0.1 C rate, the inset is the cycling performance of a Li/Se cell for comparison. (**B**) The selected discharge and charge voltage profiles.

In summary, a diphenyl trisulfide-selenium nanowire hybrid cathode is reported in this work. Because of the morphological similarity between Se nanowires and CNTs, they can form a highly conductive and interwoven composite electrode. When DPTS is introduced, an organic-inorganic hybrid electrode is assembled, which has the advantages of conductive Se and reduction of lithium polysulfides. Upon charge, the selenium radicals formed during the delithiation process are inserted in the molecular structures of DPDS and DPTS to form several diphenyl sulfoselenide compounds containing S-Se bonds. They also form dynamic bonds with sulfur separately. The results obtained from the spectroscopic and analytical techniques along with molecular dynamic analysis supply the direct evidence to validate the formation of dynamic S-Se bonds upon charge. The formation of such bonds alters the redox process of Se and reduces the formation of high-order lithium polyselenides. Thus, a stable battery performance of 250 cycles with high discharge capacities and Coulombic efficiencies is achieved. The effective combination of the organic material and the inorganic nanomaterial is a promising approach to develop hybrid electrodes with superior battery performance.

Acknowledgements

This work was supported by the National Natural Science Foundation of China (Grant Nos. 21975225 and 51902293), the Recruitment Program of Global Youth Experts in China, and Zhengzhou University.

Conflict of interest

The authors declare no conflict of interest.

Keywords: organic polysulfide • selenium nanowire • organic-inorganic hybrid • lithium battery

[1] a) A. Yoshino, *Angew. Chem. Int. Ed.* **2012**, *51*, 5798-5800; b) A. Manthiram, *J. Phys. Chem. Lett.* **2011**, *2*, 176-184.
[2] a) Y. Liang, Z. Tao, J. Chen, *Adv. Energy Mater.* **2012**, *2*, 742-769; b) D. Y. Wang, W. Guo, Y. Fu, *Acc. Chem. Res.* **2019**, *52*, 2290-2300.
[3] M. Wu, Y. Cui, A. Bhargav, Y. Losovyj, A. Siegel, M. Agarwal, Y. Ma, Y. Fu, *Angew. Chem. Int. Ed.* **2016**, *55*, 10027-10031.
[4] a) M. Wu, A. Bhargav, Y. Cui, A. Siegel, M. Agarwal, Y. Ma, Y. Fu, *ACS Energy Lett.* **2016**, *1*, 1221-1226; b) W. Guo, Z. D. Wawrzyniakowski, M. M. Cerda, A. Bhargav, M. D. Pluth, Y. Ma, Y. Fu, *Chem. Eur. J.* **2017**, *23*, 16941-16947.
[5] a) A. Bhargav, M. E. Bell, Y. Cui, Y. Fu, *ACS Appl. Energy Mater.* **2018**, *1*, 5859-5864; b) P. Sang, Y. Si, Y. Fu, *Chem. Commun.* **2019**, *55*, 4857-4860.
[6] C. P. Yang, S. Xin, Y. X. Yin, H. Ye, J. Zhang, Y. G. Guo, *Angew. Chem. Int. Ed.* **2013**, *52*, 8363-8367.
[7] a) X. Li, J. Liang, J. Luo, C. Wang, X. Li, Q. Sun, R. Li, L. Zhang, R. Yang, S. Lu, H. Huang, X. Sun, *Adv. Mater.* **2019**, *31*, 1808100; b) X. Chen, L. Peng, L. Wang, J. Yang, Z. Hao, J. Xiang, K. Yuan, Y. Huang, B. Shan, L. Yuan, J. Xie, *Nat. Commun.* **2019**, *10*, 1021; c) Z. Li, J. Zhang, B. Y. Guan, X. W. Lou, *Angew. Chem. Int. Ed.* **2017**, *56*, 16003-16007.
[8] Y. Wei, Y. Tao, Z. Kong, L. Liu, J. Wang, W. Qiao, L. Ling, D. Long, *Energy Storage Mater.* **2016**, *5*, 171-179.
[9] a) A. Abouimrane, D. Dambournet, K. W. Chapman, P. J. Chupas, W. Weng, K. Amine, *J. Am. Chem. Soc.* **2012**, *134*, 4505-4508; b) X. Li, J. Liang, K. Zhang, Z. Hou, W. Zhang, Y. Zhu, Y. Qian, *Energy Environ. Sci.* **2015**, *8*, 3181-3186.
[10] W. Guo, A. Bhargav, J. D. Ackerson, Y. Cui, Y. Ma, Y. Fu, *Chem. Commun.* **2018**, *54*, 8873-8876.
[11] a) S. Ren, L. Y. Chang, S. K. Lim, J. Zhao, M. Smith, N. Zhao, V. Bulovic, M. Bawendi, S. Gradecak, *Nano Lett.* **2011**, *11*, 3998-4002; b) J. Zhou, T. Qian, N. Xu, M. Wang, X. Ni, X. Liu, X. Shen, C. Yan, *Adv. Mater.* **2017**, *29*, 1701294.
[12] Y. Cui, X. Zhou, W. Guo, Y. Liu, T. Li, Y. Fu, L. Zhu, *Batteries & Supercaps* **2019**, *2*, 784-791.
[13] S. Xiong, B. Xi, W. Wang, C. Wang, L. Fei, H. Zhou, Y. Qian, *Cryst. Growth Des.* **2006**, *6*, 1711-1716.

10.1002/anie.201913243

[14] F. Li, Y. Si, B. Liu, Z. Li, Y. Fu, *Adv. Funct. Mater.* **2019**, *29, 1902223*.
[15] a) J. He, Y. Chen, W. Lv, K. Wen, P. Li, Z. Wang, W. Zhang, W. Qin, W. He, *ACS Energy Lett.* **2016**, *1*, 16-20; b) K. Han, Z. Liu, J. Shen, Y. Lin, F. Dai, H. Ye, *Adv. Funct. Mater.* **2015**, *25*, 455-463.
[16] C. A. Szafranski, W. Tanner, P. E. Laibinis, R. L. Garrell, *Langmuir* **1998**, *14*, 3570-3579.
[17] H. H. Eysel, S. Sunder, *Inorg. Chem.* **1979**, *18*, 2626-2627.
[18] J. Zhang, Y. Xu, L. Fan, Y. Zhu, J. Liang, Y. Qian, *Nano Energy* **2015**, *13*, 592-600.
[19] P. Dong, K. S. Han, J. I. Lee, X. Zhang, Y. Cha, M. K. Song, *ACS Appl. Mater. Interfaces* **2018**, *10*, 29565-29573.